Contrib Mineral Petrol (2004) 148: 69–78
DOI 10.1007/s00410-004-0586-y

ORIGINAL PAPER

Alexander Borisov · Frank Brenker · Herbert Palme

Liquidus karrooite stability and composition at reducing conditions

Received: 5 February 2004 / Accepted: 21 April 2004 / Published online: 29 July 2004

Abstract We have determined the stability of rutile and karrooite on the liquidus of pseudobinary silicate melts of anorthite–diopside eutectic composition with, in addition, of up to 32 wt% TiO_2 at one atm total pressure and at wide range of oxygen fugacities. At 1,300°C and at an fO_2 below $10^{-11.2}$ atm rutile (TiO_2) is replaced as liquidus phase by the pseudobrookite-type $MgTi_2O_5$–Ti_3O_5 solid solution with some Al in the crystal structure. The composition of karrooite was found to be strongly dependent on oxygen fugacity. Crystalline phases were identified by transmission electron microscopy (TEM). The results obtained in this study are relevant for understanding the chemistry of lunar armalcolites. Using "excess" rutile solubility at reducing conditions, we estimated the Ti^{4+}/Ti^{3+} ratio in silicate melts at 1,300°C as function of fO_2.

Introduction

The pseudobrookite or armalcolite group of minerals are Fe-, Mg-, Ti-oxides with the general formula X_2YO_5. Endmembers are pseudobrookite (Fe_2TiO_5), ferropseudobrookite ($FeTi_2O_5$) and armalcolite ($Mg_{0.5}Fe_{0.5}Ti_2O_5$). Considerable solid solution occurs between Fe^{2+}, Fe^{3+}, Mg, and Ti. Karrooite ($MgTi_2O_5$) is the Fe-free analogue of armalcolite. So far karrooite has only been reported as a phase in Ti-rich synthetic melts, but not in nature.

A. Borisov
Institute of Geology of Ore Deposits, Petrography, Mineralogy and Geochemistry, Russian Academy of Sciences, Staromonetny 35, 109017 Moscow, Russia

A. Borisov (✉) · F. Brenker · H. Palme
Institut für Mineralogie und Geochemie, Universität zu Köln, Zülpicher Strasse 49b, 50674 Köln, Germany
E-mail: borisov@min.uni-koeln.de
Tel.: +49-221-4706112
Fax: +49-221-4705199

The mineral armalcolite may accept a substantial portion of Cr, Al and Ti^{3+} in the structure. This was first discovered in high Ti-mare basalts of the Moon and the mineral is named in honor of Armstrong, Aldrin and Collins, the Apollo 11 astronauts. High Ti–silicate melts and armalcolite are of interest in lunar petrology and geochemistry. In this paper we present data on the stability of karrooite in TiO_2-rich silicate melts.

At the reducing condition of the Moon, there should be a significant fraction of total Ti in silicate melts present as Ti^{3+} (Schreiber et al. 1978). The lower valent Ti may have a strong effect on the partitioning of Ti between crystalline phases and silicate melts (e.g., Connolly and Burnett 2003). Based on the results obtained in this work, we propose a new method of estimating the Ti^{4+}/Ti^{3+} ratio in Ti-rich silicate melts.

Experimental procedures

The experiments were conducted using the loop technique in a one atm vertical tube furnace with controlled oxygen fugacity (see details in Borisov et al. 2004). Experimental conditions are listed in Table 1.

A synthetic melt of anorthite–diopside eutectic composition was chosen as a base and 32 wt% TiO_2 were added to produce rutile-saturated melts at a wide range of temperatures. In three cases (Nos. 9–11 in Table 1) 46 wt% TiO_2 were added.

Bulk compositions of experimentally produced glasses and crystalline phases were determined by EMP using a JEOL Superprobe (Universität zu Köln, Institut für Mineralogie und Geochemie). At least seven points in each glass sample were analyzed and the data were averaged. In order to identify and characterize the Mg,Ti-rich phases, which were found to replace rutile on the liquidus at reducing conditions, several run products were studied with the transmission electron microscope (TEM). Small pieces of crystals were removed from a polished sample surface. The pieces were then crushed between two glass slices to make thin fragments which

Table 1 Experimental conditions and stability of rutile and karrooite on liquidus of the melts of Di–An–TiO_2 system

No.	Sample	*t* (°C)	−log fO_2	Duration (h)	Loop	Phases
1	DAT32n	1,222	0.68	36	Pt	Rut + Gl
2	DAT32m	1,241	0.68	11	Pt	Rut + Gl
3	DAT32c	1,249	0.68	4	Pt	Rut + Gl
4	DAT32f	1,288	0.68	41	Pt	Rut + Gl
5	DAT32a	1,294	0.68	21	Pt	Rut + Gl
6	DAT32p	1,343	0.68	24	Pt	Rut + Gl
7	DAT32r	1,355	0.68	21	Pt	Rut + Gl
8	DAT32o	1,366	0.68	20	Pt	Gl
9	DAT46 h	1,398	0.68	60	Pt	Rut + Gl
10	DAT46I	1,421	0.68	20	Pt	Rut + Gl
11	DAT46j	1,450	0.68	8	Pt	Rut + Gl
12	DAT32-6	1,300	9.84	64	Pd	Rut + Gl
13	DAT32-18	1,300	10.11	68	Pt	Rut + Gl
14	DAT32-18a	[a]	[a]	[a]	Rh	Rut + Gl
15	DAT32-16	1,300	10.28	65	Pt	Rut + Gl
16	DAT32-7	1,300	10.44	65	Pd	Rut + Gl
17	DAT32-17	1,300	10.75	68	Pd	Rut + Gl
18	DAT32-17a	[a]	[a]	[a]	Pt	Rut + Gl
19	DAT32-17b	[a]	[a]	[a]	Rh	Rut + Gl
20	DAT32-11	1,301	10.99	67	Pd	Rut + Gl
21	DAT32-5	1,298	11.12[b]	65	Pd	Rut + Gl
22	DAT32-5a	[a]	[a]	[a]	Pd	Kar + Rut + Gl
23	DAT32ik[c]	1,300	11.21	15	Pt	Kar + Rut + Gl
24	DAT32jk[c]	[a]	[a]	[a]	Pt	Kar + Rut + Gl
25	DAT32-12	1,300	11.47	67	Pd	Kar + Gl
26	DAT32-12a	[a]	[a]	[a]	Pt	Kar + Gl
27	DAT32-19	1,300	11.75	66	Pt	Kar + Gl
28	DAT32-15	1,300	12.13	62	Pt	Kar + Gl
29	DAT32-15a	[a]	[a]	[a]	PtRh6	Kar + Gl
30	DAT32-15b	[a]	[a]	[a]	Ni	Kar + Gl
31	DAT32il[c]	1,281	11.50	20.5	Pt	Kar + Rut + Gl
32	DAT32jl[c]	[a]	[a]	[a]	Pt	Kar + Rut + Gl
33	DAT32 g	1,249	12.11	29	Pt	Kar + Gl
34	DAT32 h	1,220	12.32[b]	29	Pt	Rut + Sph + Gl

Rut rutile, *Gl* glass, *Kar* karrooite, *Sph* sphene (titanite)
[a]The charge was melted in the same experimental run as the sample above
[b]Calculated fO_2 (in all other reducing runs a solid electrolyt sensor was applied)
[c]Reversal experiments: initial DAT32i samples were melted in the same run with DAT32-18 and contained Rut + Gl, initial DAT32j samples were melted in the same run with DAT32-19 and contained Kar + Gl

are transparent to electrons. The crushed fragments were remounted on a carbon coated copper grid using adhesive acetone. Samples were analyzed with two analytical transmission electron microscopes (ATEM), a Philips EM400 and a Philips CM12, operating at 120 kV. Both ATEMs are equipped with energy dispersive X-ray detectors. Standard techniques like bright and dark field imaging and selected area electron diffraction (SAED) were applied. D-spacings were calculated and the SAED patterns simulated using published structure data of pseudobrookite (Grey et al. 1994).

Results and discussion

The TiO_2-containing glasses produced in experiments at reducing conditions are dark and non-transparent, compared to those produced in air which are transparent and yellow–brown. Three glasses of the DAT46 series (Nos. 9–11 in Table 1) contain substantial fractions of nontransparent poorly-quenched material. However, unfocused probe beam measurements gave similar bulk compositions for the clear glass and the non-transparent material.

The phases present in the charges are given along with experimental conditions in Table 1. The TiO_2 dissolved in the silicate melt apparently suppresses the crystallization of anorthite and diopside expected for this composition. The eutectic temperature in the Di–An system is 1,274°C, but TiO_2-rich samples crystallized only rutile even at temperatures as low as 1,222°C.

Rutile solubility in silicate melts in air

The results of the experiments on rutile solubility in air are given in Table 2 and graphically displayed in Fig. 1. With increasing temperature, from 1,222 to 1,450°C, the TiO_2 content of rutile-saturated Di–An eutectic melts increases by more than a factor of two, from 19 to 43 wt%. A second order polynomial fit (see Fig. 1) gives a solubility of 25.2 wt% TiO_2 at a temperature of 1,300°C.

In rutile saturated melts, the activity of TiO_2 is unity ($a_{TiO_2} = 1$). Because $a_{TiO_2} = \gamma_{TiO_2} \times X_{TiO_2}$, the activity coefficient of TiO_2 in silicate melts saturated with TiO_2 is: $\gamma_{TiO_2} = 1/X_{TiO_2}$.

The values of γ_{TiO_2} are also given in Table 2. Within the temperature range from 1,222 to 1,450°C, γ_{TiO_2} decreases from 6.6 to 2.8. At higher temperature the solution of TiO_2 in An–Di melts becomes increasingly ideal. These data may also be used to determine the par-

Table 2 Rutile solubility and TiO_2 thermodynamic properties in the melts of Di–A–TiO_2 system in air

No.	Sample	T (K)	TiO_2 (wt%)	X_{TiO_2}	γ_{TiO_2}	$-\Delta\bar{G}^{E}_{TiO_2}$ (kJ/mol)
1	DAT32n	1,495	19.09	0.1508	6.63	23.52
2	DAT32m	1,514	20.19	0.1601	6.24	23.06
3	DAT32c	1,522	21.28	0.1685	5.93	22.53
4	DAT32f	1,561	24.50	0.1965	5.09	21.12
5	DAT32a	1,567	25.38	0.2044	4.89	20.68
6	DAT32p	1,616	29.13	0.2383	4.20	19.27
7	DAT32r	1,628	30.12	0.2483	4.03	18.86
8	DAT46 h	1,671	35.98	0.2984	3.35	16.80
9	DAT46i	1,694	39.39	0.3281	3.05	15.70
10	DAT46j	1,723	43.05	0.3575	2.80	14.73

Experimental conditions are given in Table 1

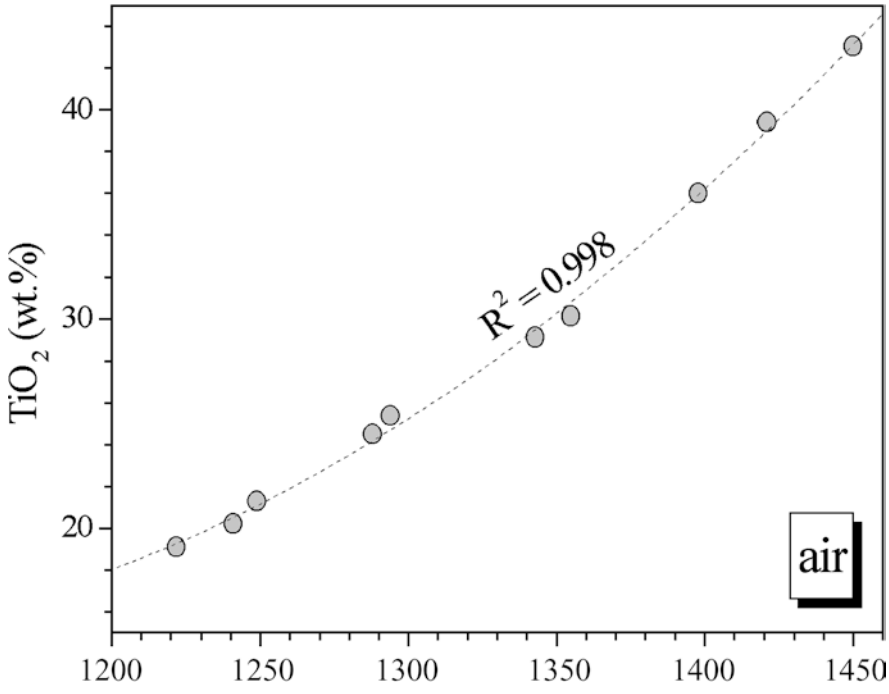

Fig. 1 Temperature dependence of the rutile solubility in An–Di eutectic melts in air Polynomial fit is shown as *dashed line*

tial molar excess Gibbs function: $\Delta\bar{G}^{E}_{TiO_2} = RT\ln\gamma_{TiO_2}$, where R is the gas constant and T is the absolute temperature. The $\Delta\bar{G}^{E}_{TiO_2}$ values are listed in Table 2 and in Fig. 2, a plot of $\Delta\bar{G}^{E}_{TiO_2}$ vs. T (K) is also presented. From the excellent correlation ($R^2 = 0.995$) a partial molar enthalpy of mixing, $\Delta\bar{H}_{TiO_2} = -81.74\pm0.23\ (1\sigma)$ kJ/mol and partial molar excess entropy of mixing, $\Delta\bar{S}^{E}_{TiO_2} = -38.84 \pm 0.98\ (1\sigma)\ \mathrm{J/(mol\,K)}$ are calculated. Using these excess functions it is possible to extrapolate to a temperature of 1,830°C where the mixing of TiO_2 with An–Di melt will be ideal.

Rutile solubility at low oxygen fugacity and estimates of the Ti^{4+}/Ti^{3+} ratio in silicate melts

The results of the rutile solubility experiments at reducing conditions and a constant temperature of 1,300°C are given in Table 3 and displayed in Fig. 3. In melts with 26.2–27.5% TiO_2 the solubilities are about 1–2 wt% higher than those found for the same temperature in air (see section above). In addition, solubilities seem to increase with decreasing fO_2.

We suggest that the higher TiO_2 concentration required to saturate a silicate melt at reducing conditions, reflects the presence of a significant fraction of Ti^{3+}. The TiO_2 content in a silicate melt in equilibrium with rutile is described by the equation: TiO_2 (rutile) = TiO_2 (melt), where the reaction constant depends on temperature but independent of oxygen fugacity. At low oxygen fugacities a certain amount of Ti^{3+} ($TiO_{1.5}$ oxide) in addition to Ti^{4+} (TiO_2 oxide) will be stable in silicate melts (see, for example, Schreiber et al. 1978). The fraction of Ti^{3+} will increase with decreasing fO_2 according to the formula:

$$\log Ti^{4+}/Ti^{3+}\ (\mathrm{melt}) = k\ \log fO_2 + A \qquad (1)$$

where $k = 1/4$ for any one-electron redox exchange reactions (Ti^{4+}/Ti^{3+}, Fe^{3+}/Fe^{2+}, Cu^{2+}/Cu^{+}, etc.) and A = constant at fixed temperatures. The lower fO_2 is the higher is $TiO_{1.5}$ and as a consequence the total titanium content of the melt increases.

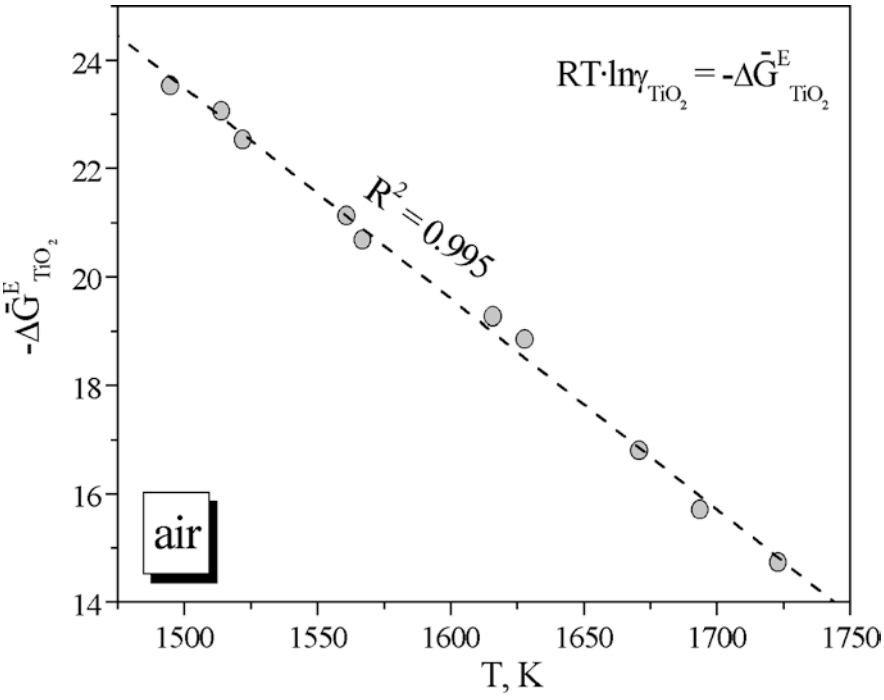

Fig. 2 Temperature dependence of $\Delta\bar{G}^{E}_{TiO_2}$ in An–Di eutectic melt

Table 3 "Excess" rutile solubility (wt%) at the reducing conditions and Ti^{4+}/Ti^{3+} ratio in Di–An–TiO_2 melts at 1,300°C

No.	Sample	–log fO_2	TiO_2	TiO_2^{ex}	Ti^{4+}/Ti^{3+} [a]
1	DAT32-6	9.84	26.29	1.06	26.39
2	DAT32-18	10.11	26.18	0.95	29.46
3	DAT32-18a	10.11	26.34	1.11	25.33
4	DAT32-16	10.28	26.63	1.40	19.97
5	DAT32-7	10.44	26.54	1.31	21.40
6	DAT32-17	10.75	26.69	1.46	19.19
7	DAT32-17a	10.75	26.69	1.46	19.14
8	DAT32-17b	10.75	26.89	1.66	16.88
9	DAT32-11	10.99	27.46	2.23	12.57
10	DAT32-5	11.12	26.99	1.76	15.91

Experimental conditions are given in Table 1, the procedure of calculation see in text

[a]Calculated from TiO_2 excess, see text for details

To calculate the Ti^{4+}/Ti^{3+} ratios of the silicate melts at low oxygen fugacity we proceeded as follows. In experiments in air we assumed all Ti as Ti^{4+} (25.2wt% TiO_2 at 1,300°C). At low oxygen fugacities, we defined an "excess" TiO_2 as $(TiO_2)_i - 25.2$, then converted this values into $TiO_{1.5}$. Finally, we calculated the ratios Ti^{4+}/Ti^{3+} (that is $TiO_2/TiO_{1.5}$) which were then used for a regression of log (Ti^{4+}/Ti^{3+}) vs. log fO_2. The values used in these calculations are listed in Table 3.

As a result, the Ti^{4+}/Ti^{3+} ratio in TiO_2-rich melts at any fO_2 may be found with reasonable accuracy ($R^2 = 0.763$) from Eq. 1 with $k = 0.22 \pm 0.04$ (1σ) and $A = 3.59 \pm 0.06$ (1σ). Although we made no assumption about k, the value obtained from the regression is close to the theoretical value of 0.25 within error limits, confirming the approach used here.

The procedure to estimate the Ti^{4+}/Ti^{3+} ratio in TiO_2 saturated silicate melts is an alternative to the chemical redox titration (Johnston 1965) or near-infrared/visible spectroscopy and the electron spin resonance with calibration via chemical redox titration described by Schreiber et al. (1978, 1982). Hanson and Jones (1998) estimated the Cr^{3+}/Cr^{2+} ratio in spinel-saturated melts using a similar procedure. These authors also assumed that the Cr^{3+} content is buffered by presence of spinel but is independent of fO_2, and the "excess" of the total Cr content at reducing conditions is due to the presence of Cr^{2+}.

Extrapolation of our data to IW-1 ($10^{-11.6}$ atm at 1,300°C), which is on average relevant to the formation of lunar rocks, yields a Ti^{4+}/Ti^{3+} ratio of about 11.5, implying that 8% of total Ti in silicate melt is Ti^{3+}. We can compare this result with published experimental data for which the temperature dependence of the Ti^{4+}/Ti^{3+} ratio is known or may be calculated. Schreiber et al. (1978) studied Ti^{4+}/Ti^{3+} in FAD (forsterite–anorthite–diopside) and FAS (forsterite–anorthite–silica) systems with trace titanium at 1,500 and 1,550°C. Johnston (1965) studied Ti-doped N2S melt ($Na_2O \cdot 2SiO_2$) at a wide temperature range. By extrapolating these data to IW-1 and 1,300°C we obtain 0.04, 0.1 and 1.2% of total Ti as Ti^{3+} in FAD, FAS and N2S melts, respectively. Thus there appears to be a large effect of melt composition on the Ti^{4+}/Ti^{3+} ratio. In addition, the total Ti content may also influence the Ti^{4+}/Ti^{3+} ratio.

So far we estimated Ti^{4+}/Ti^{3+} ratios only for a single temperature of 1,300°C. To use our data at a wider range of temperatures, we assume a temperature dependence of the Ti^{4+}/Ti^{3+} ratio. A slope of log(Ti^{4+}/

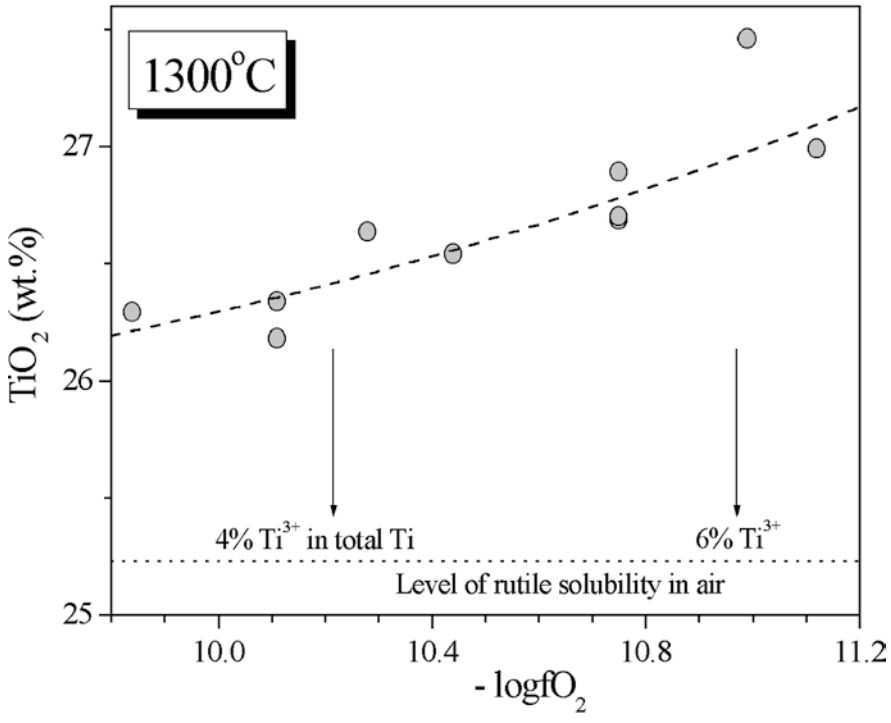

Fig. 3 Rutile solubility at reducing conditions at 1,300°C. Apparent total TiO_2 content, if $\log(Ti^{4+}/Ti^{3+}) = 0.22 \log fO_2 + 3.59$, is shown as *dashed line* (see text for details)

Ti^{3+}) vs. $1/T$ (K) was calculated from the experiments of Schreiber et al. (1978). Both slopes agree within error limits with $29{,}900 \pm 12{,}000$ for the FAS and $29{,}100 \pm 7{,}800$ for the FAD systems. Taking an average value of 29,500 the Ti^{4+}/Ti^{3+} ratio in An–Di liquids with excess TiO_2 may be calculated at any given temperature as:

$$\log Ti^{4+}/Ti^{3+}\ (\text{melt}) = 0.25 \log fO_2 + 29{,}500/T\,(\text{K}) - 14.82\ (\pm 0.06,\ 1\sigma) \qquad (2)$$

This equation will be used for calculations of Ti^{4+}/Ti^{3+} ratios in silicate melts coexisting with karrooite. We should mention, however, that the slope of $\log Ti^{4+}/Ti^{3+}$ vs. $1/T$ derived from Johnson's (1965) data for N2S melts is much lower ($6{,}400 \pm 900$, 1σ). As the data of Schreiber et al. (1978) were obtained for multicomponent melts, they may be more representative of natural silicate liquids.

Karrooite as liquidus phase and its dependence on oxygen fugacity

The liquidus phases of the pseudobinary system of Di–An eutectic composition with 32 wt% TiO_2 are shown in Fig. 4. We found that in these melts below a "critical fO_2" (about $10^{-11.2}$ atm at 1,300°C) the liquidus phase rutile is replaced by a Mg–Ti oxide phase with Ti/Mg atomic ratios varying from 2.6 to 3.3 (Table 4). The most TiO_2-rich phase in the MgO–TiO_2 binary in air is karrooite, $MgTi_2O_5$ with a Ti/Mg atomic ratio of 2 (e.g., Woermann et al. 1969). It is also known (Borowiec and Rosenqvist 1985; Grey et al. 1994) that at low fO_2 karrooite may contain Ti_3O_5 ($Ti^{3+}{}_2TiO_5$) in the structure, which results in an increase of the apparent Ti/Mg ratio. The iron-containing analogue of karrooite is armalcolite, $(Mg,Fe)Ti_2O_5$, which may also, similar to karrooite, contain a significant fraction of a Ti_3O_5 component in solid solution at strongly reducing conditions (Lindsley et al. 1974; Wechsler et al. 1976; Borowiec and Rosenqvist 1985).

The results of the TEM measurements of three representative samples support the pseudobrookite structure of the Mg–Ti-rich phases (Table 5, Fig. 5). For a comparison we used the structural data from the experimental work of Grey et al. (1994) on the solid solution of $MgTi_2O_5$ with Ti_3O_5. The sample with 25% of a Ti_3O_5 component synthesized at 1,200°C and an fO_2 of $10^{-16.2}$ atm (Table 4 in Grey et al. 1994) demonstrates the good agreement with our EPMA measurements of the unknown phase. The cell parameters and the space group used for indexing and simulating the SAED pattern are $a = 9.76$ Å, $b = 3.76$ Å, $c = 9.99$ Å and Ccmm, respectively. A comparison of calculated d-spacings and measured values (Fig. 5) shows good agreement, indicating very similar structures.

The *hkl* values are similar for all analyzed samples within error limits. High resolution TEM show a homogenous lattice spacing of 9.87 Å. SAED patterns show streaking along 001 (Fig. 2b, c) indicating a slight modulation of the structure parallel to (0 0 1). Reflections of the type $h + k =$ odd are absent (e.g. Fig. 5d) due to the C-centering of the structure.

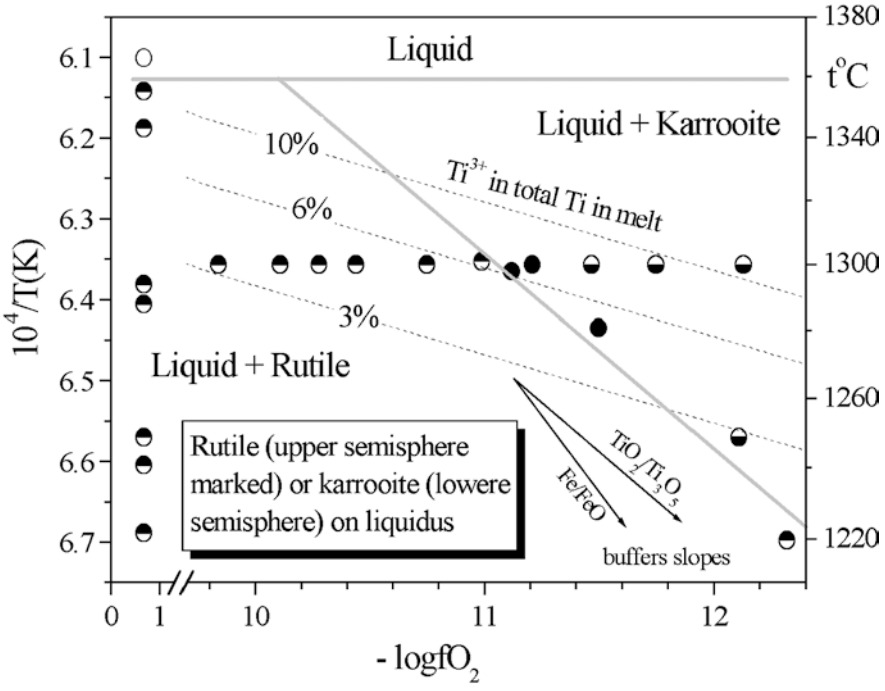

Fig. 4 Rutile/karrooite stability on the liquidus of the Di–An eutectic composition with addition of 32 wt% TiO_2. The slopes of TiO_2/Ti_3O_5 and IW equilibria are shown with *arrows*. The isopleths of Ti^{3+} content in total Ti in silicate melts are shown with as *dashed lines*

The majority of experiments were done at a temperature of 1,300°C. Thus, the temperature dependence of the fO_2 where rutile replaces karrooite as liquidus phase is not very well defined. Nevertheless, it is clear that the temperature dependence of this transition should be parallel to the TiO_2/Ti_3O_5 equilibrium (thermodynamic data from Robie et al. 1979) but not to the IW buffer line (see Fig. 4). It appears that Ti^{3+} stabilizes karrooite as liquidus phase. The fraction of Ti that is present as Ti^{3+} in the melt is according to our estimate (Eq. 2) shown in Fig. 4. When this fraction exceeds 6%, rutile is replaced by karrooite as liquidus phase. It is not clear how wide the fO_2 range is where both phases coexist, but it should not exceed 0.5 log unit (see Fig. 4).

In one-bar experiments with natural or synthetic high-titanium lunar basalts the first phases to crystallize are frequently chromite and ilmenite and not rutile (e.g., Akimoto et al. 1970; Usselmann et al. 1975). This is due to the presence of FeO in the silicate melt. The low fO_2 manifests itself in the presence of armalcolite. Usselmann et al. (1975) found, for example, that at 1,150°C armalcolite appears at fO_2 between $10^{-12.9}$ and $10^{-13.15}$ atm.

Karrooite composition as an fO_2 indicator

Stanin and Taylor (1980) demonstrated that the amount of Ti^{3+} in armalcolite may be an indicator of the oxygen fugacity at which lunar rocks crystallized. Their experiments were, however, restricted to a single temperature (1,160°C) at two different oxygen fugacities below the iron/wüstite buffer (IW-1.2 and IW-0.2). Our new data on the composition of karrooite cover a wide range of temperatures and oxygen fugacities and may thus provide new information concerning the appearance of TiO_2-rich phases in melts enriched in TiO_2.

The microprobe analyses of experimentally produced karrooites are given in Table 4. High totals, exceeding 100%, reflect a significant fraction of Ti^{3+}, as will be demonstrated later. Small fractions of CaO (0.3 wt% on average) were ignored and are not included in Table 4. Although a Ca-containing type of armalcolite is known, armalcolites are mostly free of Ca (see summary in Papike et al. 1998). The CaO contents of our karrooites vary from 0.03 to 0.68, as analyzed with the microprobe. As the highest CaO contents are characteristic of small crystals (10–20 μm) effects from secondary photon generation in neighboring phases are likely.

The microprobe analyses were recalculated in terms of three components: $MgTi_2O_5$, $Ti^{3+}{}_2TiO_5$ and Al_2TiO_5 (Table 4). Thus, some titanium was assumed to be Ti^{3+} to give the ideal formula of three cations per five oxygens. Most published data of experimentally produced armalcolites discussed in this section were recalculated in the same way, except that $FeTi_2O_5$ and Cr_2TiO_5 were added as additional components. Following the tradition (e.g., Stanin and Taylor 1980) all Cr was assumed to be trivalent. One should remember, however, that there is no evidence, that all Cr in the armalcolite structure is present as Cr^{3+}. The compositional data of armalcolites on the liquidus of TiO_2-enriched basaltic melts were also taken from Medvedev (1996). These experiments were performed at more oxidizing conditions (wüstite/magnetite buffer) than those used here and they therefore contain $Fe^{3+}{}_2TiO_5$ as an additional component.

The relatively high fraction of the Al_2TiO_5 component in the karrooites (on average $8.2 \pm 0.4\%$, 1σ) analyzed here is remarkable. The Al_2TiO_5 component is

Table 4 Microprobe analisys of Ti-rich karrooite and recalculations to the pseudobrookite components

Sample	DAT32ik	DAT32jk	DAT32-5a	DAT32-12	DAT32-12a	DAT32-19	DAT32-15	DAT32-15a	DAT32-15b	DAT32il	DAT32jl	DAT32 g
wt%												
TiO_2	81.81	81.65	81.41	82.60	82.79	82.82	84.67	84.15	84.59	80.46	81.24	81.47
Al_2O_3	4.41	4.21	4.25	4.21	4.35	4.02	4.02	3.84	3.85	4.20	4.07	3.75
MgO	14.89	15.10	15.44	14.67	14.77	14.21	13.25	13.48	13.19	15.58	15.87	15.20
Total	101.10	100.96	101.10	101.49	101.91	101.06	101.93	101.48	101.63	100.24	101.18	100.42
Mole fractions												
Ti_2O_3	0.0595	0.0566	0.0513	0.0653	0.0640	0.0731	0.0925	0.0882	0.0938	0.0469	0.0455	0.0562
TiO_2	0.6362	0.6377	0.6395	0.6347	0.6349	0.6324	0.6258	0.6277	0.6257	0.6410	0.6419	0.6389
Al_2O_3	0.0319	0.0303	0.0303	0.0306	0.0314	0.0296	0.0301	0.0288	0.0290	0.0300	0.0287	0.0271
MgO	0.2724	0.2754	0.2789	0.2694	0.2697	0.2648	0.2516	0.2554	0.2515	0.2820	0.2839	0.2778
Pseudobrookite components, mole fractions												
$MgTi_2O_5$	0.749	0.760	0.774	0.738	0.739	0.720	0.672	0.686	0.672	0.786	0.793	0.769
Al_2TiO_5	0.088	0.084	0.084	0.084	0.086	0.081	0.081	0.077	0.077	0.084	0.080	0.075
$Ti^{3+}{}_2TiO_5$	0.163	0.156	0.142	0.179	0.175	0.199	0.247	0.237	0.251	0.131	0.127	0.156
Some important ratios												
Ti/Mg, at.	2.8	2.7	2.7	2.8	2.8	2.9	3.2	3.1	3.2	2.6	2.6	2.7
D^{Al} wt.	0.39	0.37	0.39	0.39	0.40	0.35	0.35	0.34	0.35	0.36	0.35	0.32
$D^{Ti^{3+}}$ at.[a]	8.2	7.7	7.8	7.7	7.6	8.0	8.5	8.2	8.5	9.9	9.7	23.3

Experimental conditions are given in Table 1

[a] Ti^{4+}/Ti^{3+} ratio in melt was calculated with Eq. 2 (see text for details)

Table 5 Comparison between calculated and measured d-values for karrooite from representative experimental charges

Sample	dat 32ik	dat 32-12a	dat 32-15a	Comparison
Ti_3O_5	15.4	20.0	26.8	25.0
h k l				
0 0 1	9.89	9.89–10.03	9.89–10.03	9.99
0 0 2	4.95	4.95–5.02	5.01	5.00
2 0 0	4.6–4.88	4.82–4.88	4.64–4.82	4.88
2 0 1	4.42	4.37–4.42	4.37	4.39
1 1 0	3.51–3.65	3.48–3.51	3.51–3.65	3.51
2 0 2		3.45	3.45–3.48	3.49
0 0 3	3.30	3.30–3.33	3.30–3.33	3.33
1 1 1	3.31–3.33	3.27–3.31	3.3	3.31
1 1 2		2.94	2.89	2.87
2 0 3	2.77	2.74	2.69	2.75

Experimental conditions are given in Table 1, sample for comparison (Grey et al. 1994) was synthesized at 1,200°C and $fO_2 = 10^{-16.2}$ atm

independent of temperature and oxygen fugacity, The armalcolites produced in the experiments of Stanin and Taylor (1980) and O'Hara (2000) at a temperature range of 1,140–1,180°C have much lower mole fractions of the Al_2TiO_5 component ($4.4 \pm 0.3\%$, average of 29 analyses), but they are also independent of oxygen fugacity. The data of Medvedev (1996) for armalcolites produced at a temperature range of 1,200–1,300°C show an intermediate content of the Al_2TiO_5 component ($5.8 \pm 1.1\%$, average of 11 analyses), In terms of Al-partition coefficients between the crystalline phase and silicate melt (D^{Al}, wt. ratio) the difference between the first two data sets are roughly a factor of two: 0.37 ± 0.2 for the karrooites obtained in this study and 0.20 ± 0.1 for armalcolites of Stanin and Taylor (1980) and O'Hara (2000). It is not clear, whether solely the lower temperature is responsible for the lower D^{Al} values of armalcolites in comparison with karrooites or if the presence of iron in crystalline phase is also important. Additionally, the Al_2O_3 activity in silicate melts must be an important factor. For example, D^{Al} values between pseudobrookite and rhyolitic liquids at a fixed temperature of 1,400°C in air, calculated from experimental data of Gwinn and Hess (1989) vary by a factor of 20, from 0.06 for strongly peralkaline melts up to 1.1 for strongly peraluminous ones. Summarizing the discussion on aluminum in armalcolites: it is, clear that the results of studies in the melt-free "pure" armalcolite system (MgO–FeO–TiO_2 ternary) cannot be directly applied to natural systems, which always contain some Al.

However, the most variable component in the karrooites studied here is not Al_2TiO_5 but $Ti^{3+}{}_2TiO_5$, which is shown in Fig. 6. The Ti_3O_5 content in karrooite increases roughly by a factor of two, from 14 to 25%, with log fO_2 decreasing from −11.1 to −12.1 (at a fixed temperature of 1,300°C). For experimentally produced samples we can also calculated the fraction of Ti^{3+} in the coexisting melt using Eq. 2 and further the Ti^{3+} partition coefficients between karrooite and silicate melt ($D^{Ti^{3+}}$). We found the partition coefficient

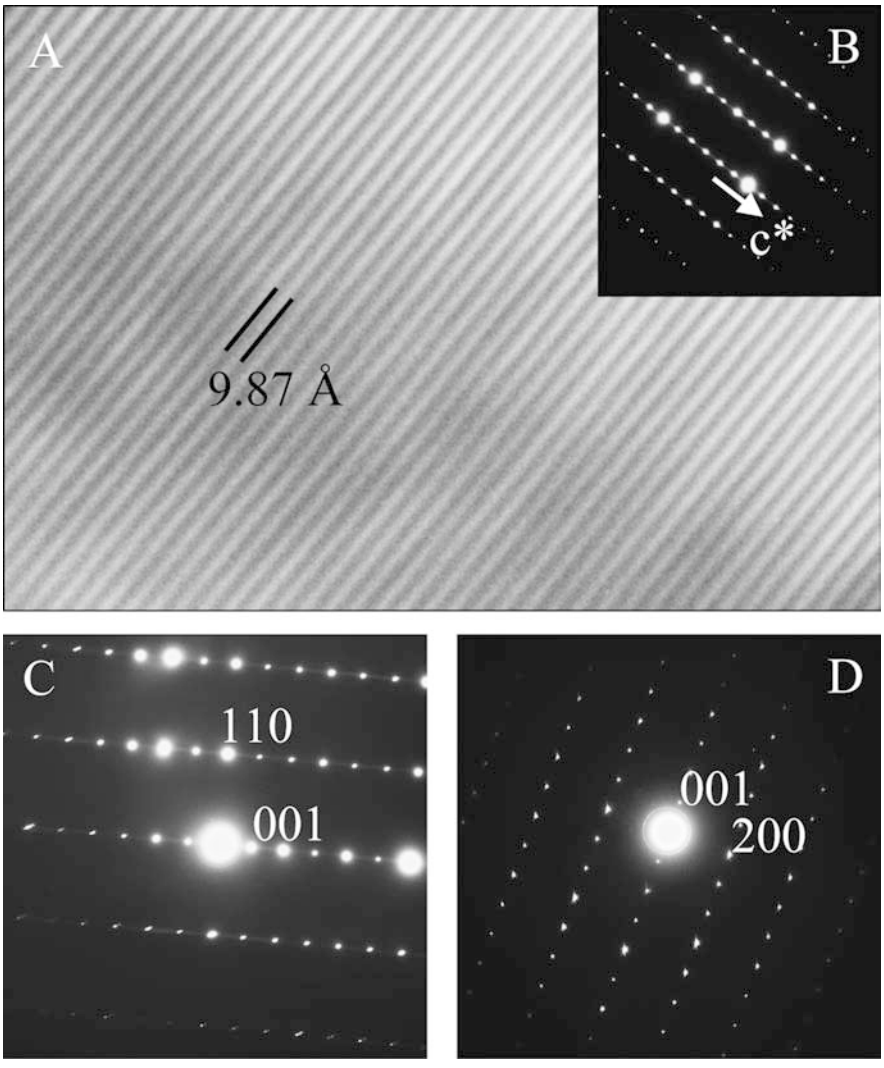

Fig. 5 a, b High resolution TEM micrograph of lattice fringes of the pseudobrookite solid solution type phase and reoriented SAED pattern of the same region viewed parallel [−110]. **c, d** SAED pattern viewed parallel [−110] and [010], respectively. The streaking parallel c* in **b** and **c** is probably due to slight modulation of the structure parallel (0 0 1)

$D^{Ti^{3+}} = 8.0 \pm 0.4$ at a constant temperature of 1,300°C to be independent of fO_2, indicating that the Ti^{3+} content of the silicate melt controls the composition of coexisting karrooite.

These results may also be represented in a slightly different way. A regressions of log $X_{Ti_3O_5}$ vs. log fO_2 and $1/T$ (K) for all karrooites studied here yields the relationship ($R^2 = 0.93$):

$$\log X_{Ti_3O_5}\ (\text{karrooite}) = -0.23 \log fO_2 - 10,844/T(\text{K}) - 3.476 \quad (3)$$

This equation can be rearranged to obtain isopleths of Ti_3O_5 contents in karrooite in log fO_2–$1/T$ coordinates:

$$\log fO_2 = -46,800/T(\text{K}) - 15.0 - 4.3 \log X_{Ti_3O_5}\ (\text{karrooite}) \quad (4)$$

There are important conclusions following from last two equations. The karrooite composition may be an oxygen fugacity indicator, with $\Delta \log fO_2 \approx 4\Delta \log X_{Ti_3O_5}$ at a fixed temperature. If the temperature is not defined, one needs a conventional redox equilibrium for comparison. It is very common in geochemistry to compare redox conditions with the IW solid buffer (or NiNiO or QFM that is, actually, interconvertible, while all three have more or less similar temperature slopes of log fO_2 vs. $1/T$ of about 25,600 ± 1,200). However, the calculations of redox conditions relative to the IW buffer will be incorrect in the case with karrooite composition. The slope of Ti_3O_5 isopleths of 46,800 ± 6,500 is equal to the slope of 41,000 of TiO_2/Ti_3O_5 equilibrium (thermodynamic data from Robie et al. 1979). In the previous section, we demonstrated that the rutile/karrooite boundary is parallel TiO_2/Ti_3O_5 but not to the IW equilibrium line.

In the case of natural armalcolites additional complications arise from the presence of iron and, especially, chromium, because the Cr^{3+}/Cr^{2+} ratio in silicate melts is also fO_2 dependent (e.g., Schreiber and Haskin 1976). We believe that the restricted experiments by Stanin and Taylor (1980) are not sufficient to correctly use armalcolite's Ti_3O_5 content as an oxygen fugacity indicator.

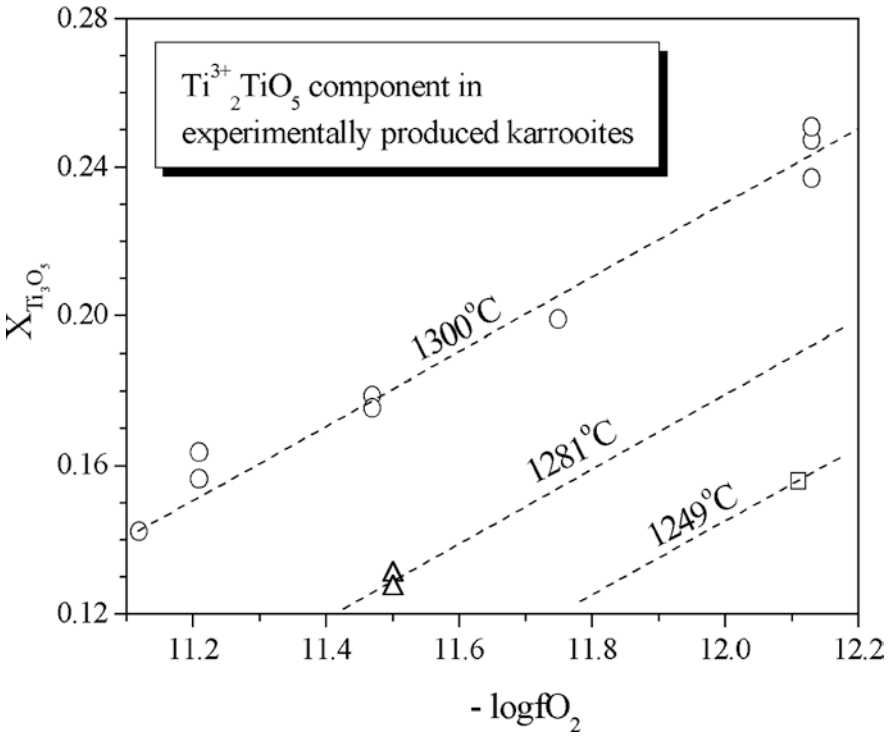

Fig. 6 The content of the Ti_3O_5 component of karrooites. *Dashed lines* for experiments at 1,300°C are from a regression (see text for details), the two other lines are parallel

Additional calibrations of armalcolite chemistry are needed at a wide *T*-fO_2 range and with special emphasis on equilibrium melt composition.

Conclusions

1. The rutile solubility in Di–An eutectic melts was determined in air at a wide range of temperatures and was found to be 25.2 wt% TiO_2 at 1,300°C.
2. At low oxygen fugacities more TiO_2 can be dissolved as some fraction of Ti is present as Ti^{3+}. This "excess" rutile solubility was used to estimate the Ti^{4+}/Ti^{3+} ratio in silicate melts at 1,300°C as function of fO_2.
3. The rutile/karrooite boundary on the liquidus of An–Di melts oversaturated with TiO_2 was determined. It was shown that the Ti_3O_5 content in karrooite is a function of the Ti^{3+} content in equilibrium silicate melts.

Acknowledgements This study was supported by the Deutsche Forschungsgemeinschaft (DFG) and by the Russian Foundation for Basic Research (project 02-05-64192).

References

Akimoto S-I, Nishikawa M, Nakamura Y, Kushiro I, Katsura T (1970) Melting experiments of lunar crystalline rocks. In: Proceedings of the Apollo 11 lunar science conference, pp 129–133

Borisov A, Lahaye Y, Palme H (2004) The effect of TiO_2 on Pd, Ni and Fe solubilities in silicate melts. Am Min 89:564–571

Borowiec K, Rosenqvist T (1985) Phase relations and oxygen potentials in Fe–Ti–Mg–O system. Scan J Met 14:33–43

Connolly HC Jr, Burnett DS (2003) On type B CAI formation: experimental constraints on fO_2 variations in spinel minor element partitioning and reequilibration effects. Geochim Cosmochim Acta 67:4429–4434

Grey IE, Li C, Madsen IC (1994) Phase-equilibria and structural studies on the solid solution $MgTi_2O_5$–Ti_3O_5. J Solid State Chem 113:62–73

Gwinn R, Hess PC (1989) Iron and titanium solution properties in peraluminous and peralkaline rhyolitic liquids. Contrib Mineral Petrol 101:326–338

Hanson B, Jones JH (1998) The systematics of Cr^{3+} and Cr^{2+} partitioning between olivine and liquid in the presence of spinel. Am Min 83:669–684

Johnston WD (1965) Oxidation–reduction equilibria in molten $Na_2O{\cdot}2SiO_2$ glass. J Am Ceramic Soc 48:184–190

Lindsley DH, Kesson SE, Hartzman MJ, Cushman MK (1974) The stability of armalcolite: experimental studies in the system MgO–Fe–Ti–O. In: Proceedings of the 5th lunar science conference, pp 521–534

Medvedev AY (1996) Synthetic armalcolite and pseudobrookite. Min Mag 60:347–353

O'Hara MJ (2000) Flood basalts, basalt floods or topless Bushvelds? Lunar petrogenesis revisited. J Petrol 41:1545–1651

Papike JJ, Ryder G, Shearer CK (1998) Lunar samples. In: Papike JJ (ed) Planetary materials. Reviews in mineralogy, vol 36. pp 5-1–5-234

Robie RA, Hemingway BS, Fisher JR (1979) Thermodynamic properties of minerals and related substances at 298.15 K and 1 bar (10^5 pascals) and at higher temperatures. U. Geol Surv Bull 1452

Schreiber HD, Haskin LA (1976) Chromium in basalts: experimental determination of redox states and partitioning among synthetic silicate phases. In: Proceedings of the 7th lunar science conference, pp 1221–1259

Schreiber HD, Thanyasiri T, Lach JJ, Legere RA (1978) Redox equilibria of Ti, Cr, and Eu in silicate melts: reduction potentials and mutual interactions. Phys Chem Glasses 19:126–139

Schreiber HD, Balazs GB, Shaffer AP, Jamison PL (1982) Iron metal production in silicate melts through the direct reduction of Fe(II) by Ti(III), Cr(II), and Eu(II). Geochim Cosmochim Acta 46:1891–1901

Stanin FT, Taylor LA (1980) Armalcolite: an oxygen fugacity indicator. In: Proceedings of the 11th lunar science conference, pp 117–124

Usselmann TM, Lofgren GE, Donaldson CH, Williams RJ (1975) Experimentally reproduced textures and mineral chemistries of high-titanium mare basalts. In: Proceedings of the 6th lunar science conference, pp 997–1020

Wechsler BA, Prewitt CT, Papike JJ (1976) Chemistry and structure of lunar and synthetic armalcolite. Earth Planet Sci Lett 29:91–103

Woermann E, Brenzny B, Muan A (1969) Phase equilibria in the system MgO - iron oxide - TiO_2 in air. American Journal of Sciences 267A:463–479